



HAL
open science

Multi-angle near infrared spectroscopy associated with common components and specific weights 5 analysis for in line monitoring

Maud Rey-Bayle, Ryad Bendoula, N. Caillol, Jean-Michel Roger

► **To cite this version:**

Maud Rey-Bayle, Ryad Bendoula, N. Caillol, Jean-Michel Roger. Multi-angle near infrared spectroscopy associated with common components and specific weights 5 analysis for in line monitoring. *Journal of Near Infrared Spectroscopy*, 2019, 27 (2), pp.134-146. 10.1177/0967033519830062 . hal-02182372

HAL Id: hal-02182372

<https://ifp.hal.science/hal-02182372>

Submitted on 12 Jul 2019

HAL is a multi-disciplinary open access archive for the deposit and dissemination of scientific research documents, whether they are published or not. The documents may come from teaching and research institutions in France or abroad, or from public or private research centers.

L'archive ouverte pluridisciplinaire **HAL**, est destinée au dépôt et à la diffusion de documents scientifiques de niveau recherche, publiés ou non, émanant des établissements d'enseignement et de recherche français ou étrangers, des laboratoires publics ou privés.

1
2
3
4 **1 Corresponding Author:**
5

6
7
8 2 Maud Rey-Bayle, IFP Energies nouvelles, Rond-point de l'échangeur de Solaize, 69360 Solaize, France
9

10
11 3 Email: maud.rey-bayle@ifpen.fr
12

13
14 **4 Multi-angle near infrared spectroscopy associated with common components and specific weights**
15
16 **5 analysis for in line monitoring**
17
18

19
20
21
22
23 6
24 7 M. Rey-Bayle^a, R. Bendoula^b, N. Caillol^c, and J-M. Roger^b
25

26 8 ^aIFP Energies nouvelles, Rond-point de l'échangeur de Solaize, BP3, 69360, Solaize, France
27

28 9 ^b ITAP, Irstea, Montpellier SupAgro, University of Montpellier, Montpellier, France
29

30
31 10 ^cAXEL'ONE, Rond-point de l'échangeur de Solaize, 69360, Solaize, France
32

33
34
35
36
37
38
39 13 **Abstract**
40

41
42 14 Near infrared (NIR) spectroscopy offers a number of important advantages for process monitoring. In
43
44 15 addition to its numerous practical advantages, an important reason to use NIR spectroscopy for process
45
46 16 monitoring is its ability to supply versatile and multivariate information. However, in heterogeneous samples
47
48 17 the interaction of light is complex and includes transmission, absorption and scattering simultaneously which
49
50 18 all affect spectra. The measurement of the signal at one point may be insufficient. A solution is to measure the
51
52 19 medium at several points and to use specific multivariate analysis.
53

54
55
56 20 In our study we propose to associate multipoint measurements with a Common Components and Specific
57
58 21 Weight Analysis (CCSWA). We monitored two media online by angular multipoint Near infrared (NIR)
59
60

1
2
3 22 spectroscopy. For the first medium, in which only the scattering varies over time, the precipitation of silica
4
5 23 was chosen to illustrate such a medium. For the second medium, both scattering and absorption vary,
6
7 24 whereby microemulsions implemented for enhanced oil recovery illustrate this medium. The results showed,
8
9 25 by combining multi-angle measurements to CCSWA, the interest of measuring at different angles. In the first
10
11 26 case, two scattering regimes have been identified and it was possible to access the anisotropy coefficient
12
13 27 during the silica precipitation reaction. In the second case study, on microemulsions, it was possible to
14
15 28 identify the different phases, and to separate the phenomena related to absorption and those related to
16
17 29 diffusion.
18
19
20

21
22 30 These encouraging results validate the interest of coupling multi-angle measurements with multivariate
23
24 31 multiblock analysis tools.
25
26
27
28

29 33 Keywords

30 34 Near infrared spectroscopy, multipoint, multi-angle, common components specific weights analysis, in line,
31
32 35 monitoring, silica, EOR, microemulsions
33
34
35
36
37

38 36

39 41 Introduction

40
41 38 Process control is a topic of increasing research in recent years ¹ in the chemical industry and, is now even
42
43 39 regulated for the pharmaceutical industry ². As mentioned by Kessler et al ³ “cost, pressure, globalization and
44
45 40 quality assurance will undoubtedly stimulate significant demand for process analytical technology (PAT)”.
46
47 41 PAT, aims to give a better scientific understanding of manufacturing process, which leads to knowledge-
48
49 42 based production. This implies the monitoring of operating parameters, such as pressure, temperature or flow
50
51 43 rates, but also physicochemical parameters as compositions, concentrations or particle sizes.
52
53
54
55
56
57
58
59
60

1
2
3 44 Spectroscopic techniques, such as near infrared (NIR) spectroscopy, have proven useful in process control for
4
5 45 several years and many uses attest of their high efficiency ⁴⁻⁷. Near infrared spectroscopy offers a number of
6
7 46 important advantages for inline analysis ⁸⁻⁹. It is a nondestructive method, requiring minimal or no sample
8
9 47 preparation, it is fast, and can be carried out without contact. Its implementation online is simple, and signal
10
11 48 transport using optical fibers offers the advantage of relocating the analyzer away from hazardous areas.
12
13
14 49 Besides the practical advantages, an important reason for using NIR spectroscopy for process monitoring is
15
16 50 its ability to supply versatile and multivariate information. Indeed, NIR spectroscopy is based on the principle
17
18 51 of light interaction with matter allowing to obtain qualitative and quantitative physical and chemical
19
20 52 information.
21
22

23
24 53 In combination with multivariate data analysis the spectral information can be correlated to product
25
26 54 properties, as it has been done for a large number of applications in various fields. For instance:

- 27
28 55 • Qualitative monitoring can be done such as on wet agglomeration of wheat flour ¹⁰, the conversion of
29
30 56 a monomer during a polymerization reaction ¹¹⁻¹², to verify that a product is in specification by
31
32 57 comparing it to reference spectra ¹³ or to follow the structural modifications of a medium and detect
33
34 58 the formation of a homogeneous gel as in the study of Mas et al. ¹⁴ for example.
35
36
37 59 • In combination with multivariate data analysis NIR spectroscopy can be used for quantitative
38
39 60 monitoring of various chemical concentrations such as glucose ^{15,16}, paracetamol ¹³, lactose ¹⁷,
40
41 61 moisture content ^{13,10}, or the quantification of heavy products in oil ¹⁸, but also for physical properties
42
43 62 like particle size^{11, 19-23}.

44
45
46 63 However, in heterogeneous samples, the interaction of light with matter is complex and spectra contain
47
48 64 combinations of the effects of transmission, absorption and diffusion ²⁴. Generally, as the chemical
49
50 65 information is sought, it is usual to correct for the scattering effects by means of empirical pretreatments ²⁵.
51
52
53 66 But in the case of PAT, there is an interest to exploit the full potential of the spectral information and use both
54
55 67 absorbance (which describes the chemistry) and scattering (which describes physicals properties as particle
56
57
58
59
60

1
2
3 68 size, agglomeration, porosity) information. However heterogeneous systems cannot be fully characterized by
4
5 69 a single measurement.
6

7
8 70 Recently, some studies focused on the use of multipoint measures for monitoring in situ heterogeneous
9
10 71 systems. Scheibelhofer et al ²⁶ have combined multipoint NIR measurements with Monte Carlo simulation to
11
12 72 understand the behavior of light in pharmaceutical tablets. Boiret and Chauchard ²⁷ have combined multipoint
13
14 73 measurements in reflection with chemometrics tools, such as partial least squares (PLS) regression and
15
16 74 principal component analysis (PCA), to predict sample hardness and active pharmaceutical ingredient (API)
17
18 75 distribution within tablets respectively. The association of PLS regression with multipoint reflection measures
19
20 76 has also shown good results for quantifying proteins and fat in milk ²⁸, to predict the fat and moisture content
21
22 77 of meat ²⁹, for in-line moisture content analysis during freeze-drying ³⁰, or for in-situ estimation of
23
24 78 concentration and particle size in colloidal suspensions ³¹. In the study by Igne et al. ³², a traditional single-
25
26 79 point NIR measurement was compared with that of a spatially resolved spectroscopic (SRS) measurement for
27
28 80 the determination of tablet assay by applying PLS regression also. Multipoint measurements have been shown
29
30 81 to be more sensitive to tablet heterogeneity, even if the authors stated that multivariate multiblock analysis
31
32 82 may further enhanced those.
33
34
35
36

37
38 83 Indeed, there would be an interest in associating multipoint measurements with specific multivariate data
39
40 84 analysis methods, like common components specific weights analysis (CCSWA) ³³. CCSWA, also known as
41
42 85 ComDim, is a multiblock analysis which makes it possible to analyze simultaneously several data matrices,
43
44 86 considering them as blocks, and to extract the information that is common among them. Historically, this
45
46 87 method was developed by Qannari et al. ³³⁻³⁶ in order to analyze tables as part of sensory assessments.
47
48 88 CCSWA has since been used to study samples analyzed on different instruments, to find relationships
49
50 89 between tables and to discriminate samples on the basis of the global information included in all tables. For
51
52 90 example Ammari et al. ³⁷ has studied the recognition of geological material by means of laser induced
53
54 91 spectroscopy, coupled with three different spectrometers. They used CCSWA to analyze jointly the signals
55
56 92 delivered by the three devices and to retrieve the best wavelength regions. In Kulmyrzaev et al. ³⁸, CCSWA
57
58
59
60

1
2
3 93 was used to investigate changes in cheeses mixing rheology, infrared spectroscopy and front-face
4
5 94 fluorescence spectroscopy. This technique has also been successfully used to show that there is a correlation
6
7
8 95 between particle size distribution and wheat flour NIR spectra ³⁹.
9
10 96 In the present paper, CCSWA coupled with multi-angle spectra measurements is proposed as a novel method
11
12 97 to monitor in situ heterogeneous systems. Two heterogeneous systems are studied in this article. One where
13
14 98 only the scattering varies, and another where the absorption and the scattering both change.
15
16 99 The silica precipitation reaction was chosen to illustrate the environment where only the scattering varies ⁴⁰.
17
18 100 The manufacture of silica is a high-stakes industrial application because silica is a product with added value
19
20 101 which can be used for many applications in various fields. The precipitation reaction stage is a crucial step in
21
22 102 the silica production chain as the main characteristics of the final product depend on it. From these
23
24 103 characteristics depend the uses of the silica produced. It is then essential to understand the mechanisms of this
25
26 104 reaction and to follow it online.
27
28 105 The monitoring of processes to improve oil extraction was chosen to illustrate a situation where the
29
30 106 absorption and the scattering both vary. The enhanced oil recovery (EOR) process involves injecting a saline
31
32 107 solution containing surfactants into the rock. With this formulation, microemulsions are formed with the oil
33
34 108 and extraction yields are improved. However, obtaining microemulsions is critical and depends on many
35
36 109 parameters such as the nature of oil, the nature of the rocks or surfactants. Depending on these parameters,
37
38 110 microemulsions with different physicochemical characteristics can be obtained. It is therefore essential to
39
40 111 understand what happens in microemulsions, to identify the type of system created and to monitor in real time
41
42 112 to ultimately optimize the process.
43
44
45
46
47
48

49 113 This paper is organized as follows. First, experimental set up are described for both studies. Then, the
50
51 114 CCSWA is presented. Results are discussed in two parts: one from the silica precipitation study, and the other
52
53 115 from the microemulsions study.
54
55

56 116

57
58
59 117 Materials and methods
60

1
2
3 118 Study 1: Silica precipitation monitoring
4
5

6 119 Material
7

8
9 120 A specially designed probe (Sam-Flex, from Indatech, Chauvin Arnoux, France) was used for spectral
10
11 121 measurements. It was composed of 5 positions for spectral measurements at 5 different angles, 3 in
12
13 122 transmission at 150° from the incoming beam, 170° and 180°, and 2 in reflection at 30° and 90°. The diagram
14
15 123 of the probe is represented in Figure 1. The air-gap of the probe was 3 mm which correspond to the optical
16
17 124 path. The probe was connected to a spectrometer (Hy-ternity, Indatech, France) composed of an NIR camera
18
19 125 equipped with an InGaAs detector (340 * 256 pixels) allowing the simultaneous measurement of all spectra.
20
21 126 Spectral data were measured in the wavelength region from 950 to 1650 nm at 5 nm intervals.
22
23
24
25
26

27 128 (i.e. "[insert Figure 1.]")
28

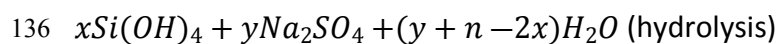
29
30 129 Figure 1: Multiangle probe diagram (Sam-Flex, Indatech)
31
32

33 130
34

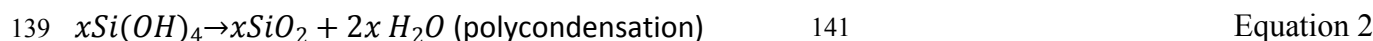
35 131 Experimental setup
36

37 132 Silica was prepared by neutralization of a sodium silicate solution (water glass) with sulfuric acid according
38
39 133 to Equation 1 and Equation 2.
40
41

42 134
43



49 138
50



54 140
55

56 142 During the reaction Si–O–Si siloxane bonds have formed basic units of inorganic polymer. Spherical
57
58 143 structures of approximately ten monomers, named nuclei, were formed and then grew to between 5 and 40
59
60

1
2
3 144 nm to form so-called elementary particles. These particles have coalesced into aggregates that are resistant to
4
5 145 grinding or dispersion in a matrix. Aggregate dimensions can range between 50 and 500 nm. At one specific
6
7 146 moment in the reaction, the gel point, the entire volume has aggregated to form a continuous gel. Finally,
8
9 147 because of a shear stress created continuously in the reaction medium, new aggregates of size between 0.2
10
11 and 40 μm were formed ^{41, 42}.
12
13

14
15 149 The synthesis (or batch) was carried out on a laboratory pilot in a perfectly stirred 25 L reactor. An aqueous
16
17 150 solution of sodium sulfate was prepared and introduced in the reactor. Then, sulfuric acid and sodium silicate
18
19 151 (provided by Solvay) were added alternatively according to the protocol established by the manufacturer (it is
20
21 152 not possible to itemize). Their rate flows were regulated and automatized.
22
23

24 153 The probe was installed on a fast loop to monitor the precipitation reaction. The probe head was oriented so
25
26 154 that the flow circulates in the gap. The experimental setup is represented in Figure 2.
27
28

29 155

30
31 156 (i.e. "[insert Figure 2.]")
32

33 157 Figure 2 : Experimental setup
34

35
36 158
37

38 159 Spectral acquisition
39

40
41 160 Spectra were acquired continuously with an integration time of 55 ms every 2 s. The spectra recording was
42
43 161 started at the first addition of reagents. It was stopped few minutes after the end of the reaction, when the
44
45 162 product was stable.
46

47
48 163 The I_0 reference was measured on air at angle 180° .
49

50 164 In order to compensate for the source spectrum and the internal response of the sensors, the transmission was
51
52 165 calculated at each angle according to Equation 3:
53
54

55 166
56
57
58
59
60

1
2
3
4 167 $S_m = \frac{I_m}{I_0}$ Equation 3
5

6
7 168

8
9 169

10
11 170 Where I_0 is the intensity measured on air at angle 180° and I_m is the intensity measured on the sample at
12
13 171 angle m , with $m = 30^\circ, 90^\circ, 150^\circ, 170^\circ$ and 180° .
14

15
16 172

17
18
19 173 Study 2: Micro emulsion monitoring

20
21
22 174 Material

23
24 175 A specially designed probe (Sam-Flex, from Indatech, Chauvin-Arnoux) was used for spectral
25
26 176 measurements. It was composed of 5 positions at 5 different angles, 3 in transmission at 170° from the
27
28 177 incoming beam, 175° and 180° , and 2 in reflection at 5° and 10° . The air-gap of the probe was still 3 mm.

29
30 178 The probe was connected to the same spectrometer as before
31

32
33
34 179

35
36 180 Samples

37
38 181 The operating protocol applied to prepare the samples came from the work of Fukumito et al. ⁴³. In this
39
40 182 publication, the different phases of the samples have been characterized, which makes it possible to know the
41
42 183 state of the system when reproducing the exact same protocol: aqueous phase W, or organic O, micro
43
44 184 emulsion water in oil W/O, or oil in water O/W, or oil and water M.

45
46 185 First, solutions of SDBS (Sigma Aldrich) at 140 g/L and NaCl (VWR chemicals) at 200 g/L were prepared
47
48 186 separately in flasks.

49
50
51 187 Then three different samples were made in 30 ml glass bottles by successively adding:

52
53 188 - 2 mL of the SDBS solution

189 - water and NaCl solutions. The volume of water and solution were calculated so that, in all samples,
190 there was an aqueous phase volume of 13.58 ml covering a set of salinity of 4, 32 and 64 g of NaCl /
191 L of water.

192 - Also, 0.84 mL of isobutanol (Alfa Aesar) was added and carefully mixed.

193 - Finally, 13.58 mL of decane (Alfa Aesar) was added and carefully mixed.

194 Samples were mixed gently by turning the bottles upside down and left to be equilibrated for 1 month at
195 room temperature.

196 For all 3 samples, the aqueous phases are in the lower part of the bottle and the organic phases in the upper
197 part.

199 Experimental setup

200 A specific setup was developed to analyze the phase in line, in order to simulate the outflow of coreflood[‡]
201 pilots^{44, 45}. Spectra were acquired off-contact through a quartz tube. The tube, with its internal diameter of 1
202 mm and its external diameter of 3 mm, was put in the probe air-gap. Its upper end was crimped with a
203 Swagelok fitting to seal. A non-beveled syringe needle was positioned at its lower end. The Swagelok fitting
204 was connected to a 1/16th inch PTFE tubing. The other end of the tubing was connected to a 50 ml glass
205 syringe. The syringe was installed on a syringe pump to make the sample flow. The setup is shown in Figure
206 3.

[‡] A laboratory test in which a fluid or combination of fluids is injected into a sample of rock. Objectives include measurement of permeability, relative permeability, saturation change, formation damage caused by the fluid injection, or interactions between the fluid and the rock. A coreflood is typically used to determine the optimum development option for an oil reservoir and often helps evaluate the effect of injecting fluids specially designed to improve or enhance oil recovery.

1
2
3 208 (i.e. "[insert Figure 3.]")
4
5

6 209 Figure 3 : Photograph of the experimental setup
7

8
9 210 Spectral acquisition
10

11 211 The syringe pump flow rate was set to 1 ml/min and maintained constant until 28 ml of product was pumped.
12

13 212 Spectra were acquired continuously with an integration time of 1.65 ms every second.
14

15 213 The I_0 reference was measured on the empty quartz tube for each angle.
16

17 214 In order to compensate for the light spectrum and the internal response of the sensors, the transmission was
18

19 215 calculated at each angle according to
20

21
22
23 216
24 217 Equation 4:

25
26 218 $S_a = \frac{I_a}{I_{0a}}$ 220 Equation 4
27
28

29
30 219
31

32 221 Where I_a is the intensity measured on the sample through the tube at the angle a , and I_{0a} is the intensity
33

34 222 measured on the empty tube at the angle a , with $a = 5^\circ, 10^\circ, 170^\circ, 175^\circ$ and 180° .
35

36
37 223
38

39
40 224 Multivariate analysis
41

42
43 225 Both sets of data were processed with MATLAB 2015b (The Mathworks, Natick, MA, USA).
44

45 226 Both times, the Savitzky-Golay function was performed to smooth spectra (2nd order, 13 points, no
46

47 227 derivative).
48

49
50 228 A CCSWA was applied on each data base. In both cases, the data bases were k blocks of n samples and p
51

52 229 wavelengths, here $p=201$ and $k= 5$ which corresponded to the angle number.
53

54
55 230 The objective of CCSWA is to describe simultaneously the k matrix \mathbf{X}_i observed for every n samples.
56

57 10
58
59
60

231 For each block i , the matrix \mathbf{X}_i has been centered by columns and the inertia matrix has been calculated as

$$232 \mathbf{W}_i = \mathbf{X}_i \cdot \mathbf{X}_i'$$

233 The matrix \mathbf{W}_i reflects the dispersion of the samples in the data space, for the block i . Since the number of
 234 samples was the same for all blocks, all \mathbf{W}_i matrices had the same size ($n \times n$). The common dimensions of all
 235 matrix was calculated iteratively according to ^{35, 46}:

$$236 \mathbf{W}_i = \sum_{dim=1}^d \lambda_{dim}^{(i)} \cdot \mathbf{q}_{dim} \cdot \mathbf{q}'_{dim} + \mathbf{R}_i \quad 238 \text{ Equation 5}$$

237
 239 Where d is the number of dimensions which has to be fixed, $\lambda_{dim}^{(i)}$ is the specific weight (= 'saliency') of the
 240 matrix \mathbf{X}_i in the construction of the common component \mathbf{q}_{dim} in the dimension dim , and \mathbf{R}_i the residual matrix
 241 of \mathbf{X}_i . So, each common component \mathbf{q}_{dim} is weighted by a scalar $\lambda_{dim}^{(i)}$ reflecting the contribution of the matrix
 242 \mathbf{X}_i in the construction of \mathbf{q}_{dim} ^{47, 36}.

243 The method consists in determining a common space for all k blocks, with each matrix having a specific
 244 contribution ("saliency"), $\lambda_{dim}^{(i)}$, to the definition of each dimension, \mathbf{q}_{dim} , of this common space by
 245 maximizing the variance common to all blocks.

246 Global scores, individual scores and loadings, and saliences in the construction of common dimensions were
 247 obtained by CCSWA.

248
 249 Results and discussions

250 Study 1: Silica precipitation monitoring

251 Spectral interpretation

252 Figure 4 shows spectra S_m acquired during the silica precipitation reaction. For all angles the same
 253 transmission profiles are observed. These are due to water absorption bands⁴⁸. The second overtone of the
 254 OH stretching band ($3\nu_{1,3}$) is at 970 nm, the combination of the first overtone of the OH stretching band and
 255 the OH bending band ($2\nu_{1,3} + \nu_2$) are at 1190 nm, and the first overtone of the OH stretching band ($2\nu_{1,3}$) is at
 256 1450 nm. The transmission profiles are stuck to the baseline when the signal is saturated in absorption. The
 257 optical path of 3 mm is too important to exploit the absorption band at 1450 nm.

258
 259 (i.e. "[insert Figure 4.]")

260 Figure 4 : Spectra I/I_0 at the five angles throughout the batch

261

262 CCSWA

263 Study of contributions

264 A CCSWA was applied on the batch. Table 1 presents the contributions of angles in the construction of
 265 common dimensions (= common components)

266

267 Table 1: Contribution of angles in the construction of common dimensions

	Dimension 1	Dimension 2	Dimension 3	Residuals
30°	83.2 %	10.8 %	6.0 %	0.1 %
90°	97.6 %	0.5 %	1.9 %	0.1 %
150°	99.3 %	0.6 %	0.1 %	0.05 %

170°	4.7 %	95.2 %	0.1 %	0.02 %
180°	90.2 %	9.2 %	0.6 %	0.1 %
Variance	69.6 %	30 %	0.4 %	

268

269 The explained variance and the residuals of the sum of the contributions of angles to each dimension show
 270 that three dimensions are sufficient to explain almost the entire variance of the dataset. Calculations for 2 and
 271 4 dimensions were carried out but was not considered as relevant.

272

273 The first two dimensions carry the major part of variance. All angles but 170° participate in the construction
 274 of the first dimension. Symmetrically, the second dimension mainly relies on the 170° angle. Dimension 3 is
 275 built mainly by the angle at 30° and to a lesser extent at 90°.

276

277 Study of common scores across all dimensions

278 CCSWA also provided overall scores, they are plotted against time for the three dimensions in Figure 5.

279

280 (i.e. "[insert Figure 5.]")

281 Figure 5 : Common scores for three common dimensions according to time. The dotted lines correspond to
 282 the modifications of the process, the star and the numbered strips correspond to product evolutions

283 Overall, two main types of events are observed at each dimension on Figure 5.

1
2
3 284 On the one hand, sharp slope changes are observed in all three dimensions. They are highlighted on the
4
5 285 figure by dashed lines. Thanks to the readings of the automaton from the pilot, it was possible to link these
6
7
8 286 slope changes to process actions: such as, adding or stopping sodium silicate or sulfuric acid.
9
10 287 On the other hand, general slopes with minima and / or maxima are observed on the dimensions. These
11
12 288 slopes modifications are not linked to instants of the reaction but to changes in the product. These are shown
13
14 289 in Figure 5 by the green star and the numbered frieze in the lower part. The number represent the main steps
15
16 290 of product evolution (although they are not fixed and probably are entangled as product is gradually
17
18 291 evolving from one stage to the next). They are determined based on the knowledge acquired by the
19
20 292 manufacturer and to the literature ⁴⁹⁻⁵³. Step 1 corresponds to elementary particles aggregation. At one
21
22 293 specific moment in the reaction, represented by the green star in Figure 5, the entire volume aggregates to
23
24 294 form a continuous gel. It is called the gel point. At this point, the physical structure of the medium instantly
25
26 295 changes. The moment the gel point occurs was validated by a turbidity monitoring retrospectively. During
27
28 296 step 2, because of the shear stress created continuously in the reaction medium, aggregates are formed. Then
29
30 297 during step 3, agglomerates rearrange and become denser, their internal structure is consolidated. During step
31
32 298 4, only one of the 2 reagents is added which dilutes the medium. Finally, the medium remains constant in the
33
34 299 last section.
35
36
37
38
39

300

301 Study of common scores

302 For all dimensions the scores profile is constant until the gel point, around 800 AU, with more or less noise.
303 This profile is linked to the fact that at the beginning of the reaction the medium is almost limpid and
304 contains few particles (this had been observed in a previous laboratory study ⁴⁰). Particles, if present had a
305 diameter smaller than tens of nanometers. For the studied wavelengths, the scattering that can be generated
306 by these particles is very small, and is not detected.

1
2
3 307

4
5 308 The scores profile of the second dimension show a maximum. A very strong increase is observed
6
7
8 309 simultaneously to the gel point up to about 1200 AU. In the rest of the batch, the scores decrease until they
9
10 310 stabilize at the end of the reaction. Table 1 which gives the contribution of angles in the construction of
11
12 311 dimensions showed the specialization of the angle at 170° for the construction of the second dimension. It
13
14 312 turns out that this angle is sensitive to serpentine photons. These photons are the ones that have slightly
15
16 313 scattered while maintaining their rectilinear trajectory. It is likely that this dimension is sensitive to the
17
18 314 simple scattering in the medium. This would be in line with the scores profile at the gel point and during
19
20 315 shearing. Indeed, during the gel formation, the scores increase because the gelation makes the whole sapphire
21
22 316 window and reaction medium's refractive index more homogeneous, creating an optical continuity of the
23
24 317 medium. The gel conducts the light forward. Then, when shearing the gel, more and more particles are
25
26 318 generated. There are therefore fewer serpentine photons and therefore less simple scattering, hence the
27
28 319 decrease in scores.
29
30

31
32
33 320 This sensitivity to the simple scattering has been observed on the loadings too. In the Figure 6 the loadings
34
35 321 obtained at 170° in the second component and the average spectrum of the batch are represented.
36
37

38 322

39
40
41 323 (i.e. "[insert Figure 6.]")
4243
44 324 Figure 6: Average spectrum of the batch and loadings obtained for the angle 170° in the second dimension
45

46 325

47
48
49 326 Two scattering consequences can be observed. From 1350 to 1600 nm, an absorption band is observed. It
50
51 327 correspond to water absorption band. This band is related to the optical path of the photon. In a previous
52
53 328 study⁴⁰, the absorption was considered as constant during the reaction. Therefore, a variation of the height of
54
55

1
2
3 329 the band is related to the increase of the optical path and thus to the scattering of the photons ⁵⁴. A higher
4
5 330 absorption makes the spectrum lower in this region. Consequently, the higher the diffusion, the longer the
6
7 331 optical path and the lower the spectrum. When multiplied by the positive peak of the loading, it produces a
8
9
10 332 lower score. Then, a slope is observed on loadings from 950 to 1350 nm. This part of the loading calculates
11
12 333 the general slope of the spectrum between 950 and 1350 nm. It appears as a rotation of the average spectrum.
13
14 334 This slope is connected to the scattering too ^{55, 56}. The higher the diffusion, the steeper the slope. Thus high
15
16 335 diffusion leads to low scores. Consequently, the loadings are sensitive to the diffusion of light. High scores
17
18 336 correspond to low diffusion, such as after the gel point, when the gel acts as a light guide.
19
20 337 Finally, thanks to the scores of the second dimension represented in Figure 5, it is possible to detect the gel
21
22 338 point very precisely and accurately. This aspect is very important as this gel point is critical for determining
23
24 339 the products future qualities. It shows that the second dimension is very informative and necessary to ensure
25
26 340 the monitoring of the reaction. The CCSWA therefore demonstrated the specific interest of the 170° angle to
27
28 341 monitor this manufacturing process.
29
30
31
32

33 342
34
35 343 The score profile of the first dimension increases throughout the reaction. With regard to Table 1, all angles
36
37 344 except the one at 170° participate in its construction. These angles do not detect the same type of photons.
38
39 345 Ballistic photons are detected at 180°, backscattered photons at 30° and 90° and forward scattered photons at
40
41 346 150°. This first dimension seems to represent the general scattering of the reaction medium, that is to say the
42
43 347 global propagation of photons without distinction between ballistic and scattered photons. Therefore we
44
45 348 assume that the multiple scattering in the reaction medium is represented in the first dimension
46
47
48
49
50

51 350 The scores of the third dimension show a minimum and a maximum. The decrease to reach the minimum
52
53 351 takes place in the same period as the growth to reach the maximum of the second dimension, just after the gel
54
55
56

1
2
3 352 point. At the opposite, during shearing, the scores of the third dimension increase to reach a maximum when
4
5 353 those of the second dimension decrease. Lastly, the scores decrease until they stabilize at the end of the
6
7 354 reaction. The third dimension probably represents the backscattered photons since the angles at 30° and 90°
8
9 355 contribute mainly to its construction (see Table 1). At the gel point, it has been said previously that the
10
11 356 optical continuity of the sapphire window with the reaction medium conducts to better light transmission.
12
13 357 More photons propagate forward, fewer backscatter. The decrease in the amount of backscattered photons
14
15 358 results in a decrease in the profile of the scores in the third dimension. CCSWA tends to consider the optical
16
17 359 system as a distribution of a total amount of photons. That is why, compared to the totality of photons at the
18
19 360 five angles, the number of photons detected at angles 30 ° and 90 ° decreases. Then during shearing, the
20
21 361 number of particles increases while their size decreases. This induces the increase of scores in the third
22
23 362 dimension and the decrease of scores in the second dimension. When the medium is sheared further, there is
24
25 363 a decrease in serpentine photons and an increase in backscattered multi-scattered photons. Shear causes
26
27 364 increased scattering of particles and the decrease in their size influences the direction of scattering. This is in
28
29 365 agreement with the theory¹³ demonstrating that the smaller the particle size, the less photons will tend to
30
31 366 scatter forward. The final decrease in the third dimension scores takes place in the last stage of the
32
33 367 precipitation reaction. Parallel to the formation of new particles in the medium, aggregates fill the already
34
35 368 existing agglomerates. They rearrange themselves, their internal structure is modified and more compact.
36
37 369 This modifies, both the specific surface area and thus the micro porosity and the number of hydrogen bonds¹.
38
39 370 These phenomena reduce the amount of light backscattered, hence the decrease in scores in the third
40
41 371 dimension. Even if at the same time, the multiple scattering continues to increase as shown by the scores of
42
43 372 the first dimension.
44
45 373 The third dimension seems to be clearly related to the direction of the scattering of photons in the medium
46
47 374 during the reaction.
48
49
50
51
52
53
54
55
56
57
58
59
60

375

376 Study 2: Micro emulsion monitoring

377 Samples

378 Solutions which were obtained are represented in the Figure 7.

379

380 (i.e. "[insert Figure 7.]")

381 Figure 7 : Photograph of the 3 samples for the micro emulsion application

382 The sample's number corresponds to the salinity of the aqueous phase (always the lower phase in the vials).

383 The different phases present in these 3 samples can be grouped into five classes, as described in Table 2.

384

385 Table 2: Phase classification

Salinity of the aqueous phase	64	32	4
Organic phases (upper)	1	2	2
Aqueous phases (lower)	4	4	3
Middle phases	NC	5	NC

386

387 Class 1 contains the organic phase where there is a micro emulsion of water in oil (W/O), as in sample 64,
388 which can be described as a Winsor II in the literature ⁴³.

389 Class 2 are the organic phases consisting only of decane (O), as in samples 32 and 4.

1
2
3 390 Class 3 is the aqueous phase where there is a micro emulsion of oil in water (O/W), as in sample 4, which
4
5 391 can be described as a Winsor I.
6

7
8 392 Class 4 are the aqueous phases consisting only of salt water with different concentrations of salt, as in
9
10 393 samples 64 and 32.
11

12 394 Class 5 is the middle phase (M) where there is a micro emulsion of water and oil which are only present in
13
14 395 Winsor III samples.
15

16
17 396
18
19 397 The visual inspection of the phases (Figure 7) shows that Class 2 phases are transparent and colorless. The
20
21 398 Class 1 and 3 phases seem slightly cloudy. For Class 4, sample 64 phase is transparent and colorless, but
22
23 399 sample 32 is whitish in its upper part and tends to be transparent in the lower part. Finally, the Class 5 phase
24
25 400 is whitish and cloudy throughout.
26

27
28 401 The cloudiness is probably due to the presence of micro emulsions. The medium appears whiter the more oil
29
30 402 is dispersed in the water. Therefore, micro emulsions probably generate scattering. The aqueous phase of
31
32 403 sample 32, should belong to a Class 4 and therefore not contain oil. This sample's whitish gradient is
33
34 404 probably due to a transition between the O/W micro emulsion and the pure aqueous phase.
35
36 405
37

38
39
40 406 Spectral interpretation
41

42 407 For a spectral interpretation of classes, only the mean absorption spectrum of each class for the 180° angle is
43
44 408 represented in Figure 8.
45

46
47 409
48
49 410 (i.e. "[insert Figure 8.]")
50

51
52 411 Figure 8 : Mean absorption spectra of classes
53
54
55
56

1
2
3 412 Two groups can be observed, separated by an important absorption difference at 1450 nm and their baseline.
4
5 413 A first group contains Classes 1 and 2 and a second group the Classes 3, 4 and 5.
6
7
8 414 The first group contains organic phases. The absorption bands of decane are found at 1208 nm and 1408 nm.
9
10 415 The second overtone of symmetrical and asymmetric elongations of CH₂ and CH₃ groups is observed at 1208
11
12 416 nm, while the absorption band at 1408 nm corresponds to the first overtone of the combination between the
13
14 417 symmetric and asymmetric elongations of the CH bonds in the CH₂ and CH₃ groups and the deformations of
15
16
17 418 the C-H bonds. Between the mean spectrum of Class 1 and the mean spectrum of Class 2, an absorption
18
19 419 difference is observed at the band at 1408 nm. This is the absorption of water present in the Class 1.
20
21 420 By observing the absorption bands of the mean spectra of the second group, the water absorption bands at
22
23 421 970 nm, 1190 nm and 1450 nm are found. Their identification was made for the previous application. Within
24
25
26 422 this group, the mean spectrum of Class 5 differs from the other two classes. At 1208 nm an absorption band
27
28 423 is observed, which is assigned as the absorption band of decane. The absorption at 1408 nm is not
29
30 424 observable, as it is hidden under the large water band at 1450 nm. In this wavelength range, the absorption of
31
32
33 425 water is much stronger than the absorption of decane. Between the mean spectra of Class 3 and 4, a slight
34
35 426 difference is observed on the 1450 nm band. The band seems slightly shifted to the left for the Class 4
36
37 427 spectrum. This may be due to the presence of salt in the Class 4 phases which could create a slight band
38
39 428 shift^{14, 48}. In addition, the baseline of the mean spectrum of Class 4 is higher than that of the mean spectrum
40
41 429 of Class 3. The presence of a baseline is one of the consequences of photon scattering⁴⁰. This is in line with
42
43 430 the visual observation of the samples in Figure 7, where a whitish appearance of Class 4 was observed,
44
45
46 431 probably related to scattering effects.
47
48
49 432

1
2
3 433 The observation of mean spectra shows that it is possible to identify almost all classes by NIR spectroscopy.
4
5
6 434 For each class, differences are observable at water and decane absorption bands. The goal for the next part of
7
8 435 this study is to determine if there is a gain to associate multi-angle analysis with CCSWA.
9

436

437 CCSWA

438 Study of contributions

439 A CCSWA was applied on all five classes of all 5 angles spectra.

440 Table 3 presents the contribution of angles in the construction of common dimensions.

441

442 Table 3: Contribution of angles in the construction of common dimensions

	Dimension 1	Dimension 2	Dimension 3	Residuals
5°	68.2 %	26.4 %	5.4 %	0 %
10°	69.0 %	25.5 %	5.5 %	0 %
170°	91.3 %	8.2 %	0.5 %	0 %
175°	85.7 %	10.9 %	3.4 %	0 %
180°	86.5 %	12.4 %	1.1 %	0 %
Variance	87.1 %	12.4 %	0.5 %	

443

1
2
3 444 The explained variance shows that three dimensions are sufficient to explain almost the entire variance of the
4
5 445 dataset. (With regard to residuals, we see that the contributions of each angle are distributed in the three
6
7 446 dimensions.)
8
9

10 447 All angles participate in the construction of the first dimension and predominantly those in transmission.
11
12 448 Contrary to the second dimension where the contributions of reflection angles are predominant. The third
13
14 449 dimension, is also built mainly by angles 5° and 10° with a contribution of the angle at 175° to a lesser
15
16 450 extent. The third dimension represents very little variance in comparison with the first two.
17
18

19 451

20
21 452 Study of common scores across all dimensions

22
23 453 CCSWA provided common scores. The scores obtained for each class were put end to end, to be able to
24
25 454 compare them. The 2 phases of Classes 2 and 4 being identical, only the scores of the binary samples were
26
27 455 represented. They are plotted according to the class for the three dimensions in Figure 9.
28
29

30 456

31
32
33 457 (i.e. "[insert Figure 9.]")
34
35

36 458 Figure 9 : Common scores for three common dimensions according to the class
37

38
39 459 Overall, common scores for the three dimensions show that each class has a different profile. It is already
40
41 460 possible to say that the CCSWA makes it possible to separate the different classes.
42
43

44 461

45 462 The common scores of the first dimension (shown in blue) separate three groups of classes. Classes 1 and 2,
46
47 463 then Classes 3 and 4 and finally Class 5. Classes 1 and 2 have negative scores, while Classes 3 and 4 have
48
49 464 positive scores. Those in Class 5 are positive but almost null. This dimension seems related to the presence
50
51 465 of water in the samples. Indeed Classes 1 and 2, having negative scores, are organic phases and contain little
52
53 466 or no water, while Classes 3 and 4, which have positive scores, are aqueous phases. Finally, Class 5 contains
54
55

56
57 22
58
59
60

1
2
3 467 water and oil in almost equal proportions. This observation of the scores relate to the observations made in
4
5 468 Figure 8 representing the mean spectra of Classes at 180 °. Moreover, this is in line with the individual
6
7 469 loadings of the transmission angles, shown in Figure 10, which strongly resemble the absorption spectrum of
8
9 470 water.

10
11
12 471

13
14 472 (i.e. "[insert Figure 10.]")

15
16
17 473 Figure 10: Individual loadings of transmission angles to the first dimension

18
19
20 474

21
22 475 The common scores of the second dimension allow to separate the classes within the groups identified in the
23
24 476 first dimension. Thanks to the second dimension, Class 1 differs from Class 2, and Class 3 differs from Class
25
26 477 4. Class 5 remains separate in this dimension as well. Class 5 scores are the most important, followed by
27
28 478 Class 4, Class 3 and Class 1, and Class 2 scores, which are the lowest. This order is very close to the order of
29
30 479 the baseline of the mean absorption spectra of the phases shown in Figure 8. The second dimension probably
31
32 480 is a general indication of the scattering in general of photons ²⁴.

33
34
35
36
37 481

38
39 482 The common scores of the third dimension bring together two groups of classes that had never been grouped
40
41 483 before. A first group consists of Classes 2, 3 and 5, and a second group consists of Classes 1 and 4.

42
43 484 In the first group, the commonality between classes is the presence of decane. For Classes 3 and 5, decane is
44
45 485 dispersed in water. In Class 2, only decane is present.

46
47 486 In the second group, the commonality between classes is the presence of water. In Class 1, water is dispersed
48
49 487 in decane and in Class 4, only water is present.

50
51 488 The third dimension is mainly constructed by the angles at 5 ° and 10 ° according to the Table 3.

1
2
3 489 To try to interpret the profile of the scores, the individual loadings of the angles 5° and 10° were represented
4
5 490 in the Figure 11.
6
7
8 491 (i.e. "[insert Figure 11.]")
9

10 492 Figure 11: Individual loadings of angles at 5° and 10° of the third dimension
11
12

13 493 Although these loadings are very noisy, information can still be exploited. Around 1660 nm, the beginning of
14
15 494 a hollow is observed. This hollow is the beginning of the absorption band of the first harmonic symmetrical
16
17 and asymmetrical elongations of the CH_2 and CH_3 groups of decane. This decane absorption band is much
18 495 larger than those at 1208 nm and 1408 nm and is even greater than the water absorption. It is probably the
19
20 496 presence of this band, which makes it possible to differentiate the groups in the profile of the common scores
21
22 497 in the third dimension. It may be that the third dimension is related to the presence of decane as a scattering
23
24 498 product.
25
26 499
27
28
29

30 500
31
32

33
34 501 Conclusions and perspectives
35
36

37 502 This study, implemented on two industrial applications, shows the interest of multi-angle spectral
38
39 503 measurements and their coupling to a Common Component and Specific Weight Analysis for monitoring
40
41 504 processes.
42
43

44 505
45

46 506 In the case of monitoring the precipitation of silica, where only light diffusion effect varies, CCWAS
47
48 507 associated with multi-angle NIR measurements has demonstrated the complementarity of the angles and its
49
50 508 interest for process monitoring. Thanks to the scores obtained by the CCSWA, the actions inherent to the
51
52 509 progress of the process could be identified by the different slopes breaks in the dimensions scores plot. Each
53
54 510 physicochemical modification of the reaction medium induced scattering phenomena ⁵⁷ which resulted in
55
56
57 24
58
59
60

1
2
3 511 curvatures, maxima and minima depending on the dimensions observed. It has been possible to identify a
4
5 512 multiple scattering regime, a simple scattering regime, and the preferred direction of light propagation in the
6
7
8 513 medium during the advancement of the precipitation reaction. CCSWA also confirmed the complementarity
9
10 514 of the angles for monitoring this reaction and the interest of multi-angle measurements. This first study
11
12 515 shows the interest of using this type of multivariate analysis on multi-angle spectral data.
13

14
15 516 Regarding the preliminary study about micro emulsion measurements, where both absorption and
16
17 517 scattering vary, CCSWA has allowed unequivocal identification of the different phases. At each dimension,
18
19 518 different phenomena have been observed. This is a gain for users because through this identification, it will
20
21 519 be possible to know in real time the type of medium obtained (aqueous phase W, or organic O, micro
22
23 520 emulsion water in oil W/O, or oil in water O/W, or oil and water M) without sampling and with only one
24
25 521 analytical technique. This monitoring is a real asset in the optimization of operational parameters on R & D
26
27
28 522 pilots.
29

30
31 523
32
33 524 Overall, the tests implemented have shown that it is very interesting to couple multi-angle measurements
34
35 525 with common component and specific weight analysis. Initially, this CCSWA tool was developed to analyze
36
37 526 data from sensory analyzes of different dimensions⁴⁷. But, the results obtained allowed reversion to the
38
39 527 physicochemical information of the mediums, starting from multi-angle spectral measurements having the
40
41 528 same dimension. Nevertheless, it would be interesting to explore the results of other existing tools for multi-
42
43 529 array multivariate analysis, and even to develop a specific tool for the analysis of multi-angle spectral data.
44
45
46 530 This study also shows the gain of monitoring in line processes, even when complex medium are involved.
47
48

49 531

50
51
52 532 Conflict of interest
53

1
2
3 533 The authors declare that they have no conflict of interest
4
5
6 534
7
8
9

10 535 **References**
11
12

- 13 536 1. R.W. Kessler, "Perspectives in process analysis", *J. Chemometrics*, **27**, 11 (2013).
14
15 537 2. Food and Drug Administration, *Guidance for Industry. Process Validation: General Principles and Practices* (Janvier
16
17 538 2011).
18
19 539 3. R. W. Kessler, K. Rebner and W. Kessler, eds., *Multi-Modal-Spectroscopy and Multivariate Data Analysis as a Tool*
20
21 540 *for Non-Invasive Process Analysis* (2013).
22
23 541 4. J. Workman, "A review of process near infrared spectroscopy: 1980–1994", *Journal of Near Infrared Spectroscopy*,
24
25 542 **1** (1993).
26
27 543 5. L.L. Simon, H. Pataki, G. Marosi, F. Meemken, K. Hungerbühler, A. Baiker, S. Tummala, B. Glennon, M. Kuentz, G.
28
29 544 Steele, H.J.M. Kramer, J.W. Ryzak, Z. Chen, J. Morris, F. Kjell, R. Singh, R. Gani, K.V. Gernaey, M. Louhi-Kultanen, J.
30
31 545 O'Reilly, N. Sandler, O. Antikainen, J. Yliruusi, P. Frohberg, J. Ulrich, R.D. Braatz, T. Leyssens, M. von Stosch, R. Oliveira,
32
33 546 R.B.H. Tan, H. Wu, M. Khan, Des O'Grady, A. Pandey, R. Westra, E. Delle-Case, D. Pape, D. Angelosante, Y. Maret, O.
34
35 547 Steiger, M. Lenner, K. Abbou-Oucherif, Z.K. Nagy, J.D. Litster, V.K. Kamaraju and M.-S. Chiu, "Assessment of Recent
36
37 548 Process Analytical Technology (PAT) Trends: A Multiauthor Review", *Org. Process Res. Dev.*, **19**, 1 (2015).
38
39 549 6. J. Workman, B. Lavine, R. Chrisman and M. Koch, "Process analytical chemistry", *Analytical chemistry*, **83**, 12
40
41 550 (2011).
42
43 551 7. Process column, ed., *Process Spectroscopy, moving spectroscopy from lab to line* (2003).
44
45 552 8. Y. Ozaki, "Near-Infrared Spectroscopy: Its Versatility in Analytical Chemistry", *Anal. Sci.*, **28**, 6 (2012).
46
47 553 9. D.A. Burns and E.W. Ciurczak, eds., *Handbook of near-infrared analysis*. CRC Press, USA (2008).
48
49 554 10. A. Ait Kaddour and B. Cuq, "In line monitoring of wet agglomeration of wheat flour using near infrared
50
51 555 spectroscopy", *Powder technology*, **190**, 1-2 (2009).
52
53
54
55
56
57 26
58
59
60

- 1
2
3 556 11. W.K. Silva, D.L. Chicoma and R. Giudici, "In-situ real-time monitoring of particle size, polymer, and monomer
4
5 557 contents in emulsion polymerization of methyl methacrylate by near infrared spectroscopy", *Polym Eng Sci*, **51**, 10
6
7 558 (2011).
- 8
9
10 559 12. N. Heigl, C.H. Petter, M. Rainer, M. Najam-ul-Haq, R.M. Vallant, R. Bakry, G.K. Bonn and C.W. Huck, "Near Infrared
11
12 560 Spectroscopy for Polymer Research, Quality Control and Reaction Monitoring", *Journal of Near Infrared Spectroscopy*,
13
14 561 **15**, 5 (2017).
- 15
16 562 13. Y. Roggo, P. Chalus, L. Maurer, C. Lema-Martinez, A. Edmond and N. Jent, "A review of near infrared spectroscopy
17
18 563 and chemometrics in pharmaceutical technologies", *Journal of pharmaceutical and biomedical analysis*, **44**, 3 (2007).
- 19
20 564 14. S. Mas, R. Bendoula, G. Agoda-Tandjawa, A. de Juan and J.-M. Roger, "Study of time-dependent structural
21
22 565 changes of laponite colloidal system by means of near-infrared spectroscopy and hybrid hard- and soft-modelling
23
24 566 multivariate curve resolution–alternating least squares", *Chemometrics and Intelligent Laboratory Systems*, **142**
25
26 567 (2015).
- 27
28 568 15. M. Sandor, F. Rüdinger, D. Solle, R. Bienert, C. Grimm, S. Groß and T. Scheper, "NIR-spectroscopy for bioprocess
29
30 569 monitoring & control", *BMC Proc*, **7**, Suppl 6 (2013).
- 31
32 570 16. H. Xu, B. Qi, T. Sun, X. Fu and Y. Ying, "Variable selection in visible and near-infrared spectra: Application to on-
33
34 571 line determination of sugar content in pears", *Journal of Food Engineering*, **109**, 1 (2012).
- 35
36 572 17. H. Huang, H. Yu, H. Xu and Y. Ying, "Near infrared spectroscopy for on/in-line monitoring of quality in foods and
37
38 573 beverages: A review", *Journal of Food Engineering*, **87**, 3 (2008).
- 39
40 574 18. J. Laxalde, C. Ruckebusch, O. Devos, N. Caillol, F. Wahl and L. Duponchel, "Characterisation of heavy oils using
41
42 575 near-infrared spectroscopy: optimisation of pre-processing methods and variable selection", *Analytica chimica acta*,
43
44 576 **705**, 1-2 (2011).
- 45
46 577 19. L.K.H. Bittner, N. Heigl, C.H. Petter, M.F. Noisternig, U.J. Griesser, G.K. Bonn and C.W. Huck, "Near-infrared
47
48 578 reflection spectroscopy (NIRS) as a successful tool for simultaneous identification and particle size determination of
49
50 579 amoxicillin trihydrate", *Journal of pharmaceutical and biomedical analysis*, **54**, 5 (2011).

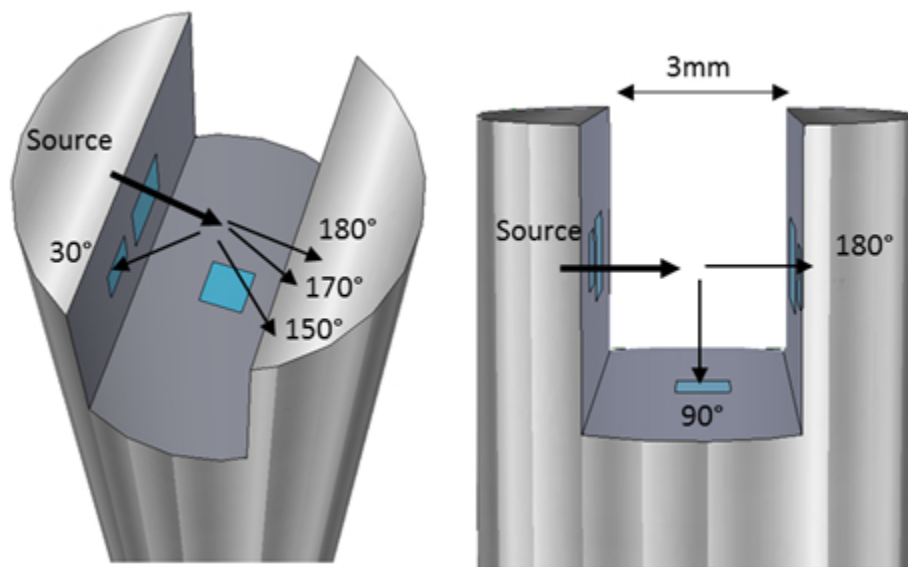
- 1
2
3 580 20. E. Prendergast, H. Abe, M. Aburada and M. Otsuka, "A Non-Destructive Method of Predicting the Particle Size of
4 the Bulk Drug Powder in an Acetaminophen Suppository by Near-Infrared Spectroscopy", *Journal of Near Infrared*
5 581 *Spectroscopy*, **20**, 2 (2012).
6
7
8 582
9
10 583 21. A.J. O'Neil, R.D. Jee and A.C. Moffat, "Measurement of the percentage volume particle size distribution of
11 powdered microcrystalline cellulose using reflectance near-infrared spectroscopyElectronic supplementary
12 584 information (ESI) available: Particle size and spectral data. See <http://www.rsc.org/suppdata/an/b3/b307263k>",
13 585 *Analyst*, **128**, 11 (2003).
14
15
16 586
17
18 587 22. R. Liu, L. Li, W. Yin, D. Xu and H. Zang, "Near-infrared spectroscopy monitoring and control of the fluidized bed
19 granulation and coating processes-A review", *International journal of pharmaceutics*, **530**, 1-2 (2017).
20
21 588
22
23 589 23. M.C. Pasikatan, J.L. Steele, C.K. Spillman and E. Haque, "Near Infrared Reflectance Spectroscopy for Online
24 Particle Size Analysis of Powders and Ground Materials", *Journal of Near Infrared Spectroscopy*, **9**, 3 (2017).
25 590
26
27 591 24. R. Bendoula, *Développements optiques pour améliorer la mesure spectrale des milieux biologiques complexes:*
28 *applications agro-environnementales. Mémoire d'habilitation à diriger des recherches* (2016).
29 592
30
31 593 25. A. Gobrecht, J.-M. Roger and V. Bellon-Maurel, "Major Issues of Diffuse Reflectance NIR Spectroscopy in the
32 Specific Context of Soil Carbon Content Estimation", in: *Advances in agronomy*, Ed by D.L. Sparks, Academic Press, an
33 594 imprint of Elsevier, San Diego, CA, pp. 145–175 (2014).
34
35
36 595
37
38 596 26. O. Scheibelhofer, P.R. Wahl, B. Larchevêque, F. Chauchard and J.G. Khinast, "Spatially Resolved Spectral Powder
39 Analysis: Experiments and Modeling", *Applied spectroscopy* (2018).
40 597
41
42 598 27. M. Boiret and F. Chauchard, "Use of near-infrared spectroscopy and multipoint measurements for quality control
43 of pharmaceutical drug products", *Analytical and bioanalytical chemistry*, **409**, 3 (2017).
44 599
45
46 600 28. A. Bogomolov, V. Belikova, V. Galyanin, A. Melenteva and H. Meyer, "Reference-free spectroscopic determination
47 of fat and protein in milk in the visible and near infrared region below 1000nm using spatially resolved diffuse
48 601 reflectance fiber probe", *Talanta*, **167** (2017).
49 602
50
51
52
53
54
55
56
57
58
59
60

- 1
2
3 603 29. Y. Dixit, M.P. Casado-Gavalda, R. Cama-Moncunill, P.J. Cullen and C. Sullivan, "Challenges in Model Development
4 for Meat Composition Using Multipoint NIR Spectroscopy from At-Line to In-Line Monitoring", *Journal of food science*,
5 604
6
7 605 **82**, 7 (2017).
8
9
10 606 30. A. Kauppinen, M. Toiviainen, M. Lehtonen, K. Järvinen, J. Paaso, M. Juuti and J. Ketolainen, "Validation of a
11
12 607 multipoint near-infrared spectroscopy method for in-line moisture content analysis during freeze-drying", *Journal of*
13
14 608 *pharmaceutical and biomedical analysis*, **95** (2014).
15
16 609 31. Y.-C. Chen, D. Foo, N. Dehanov and S.N. Thennadil, "Spatially and angularly resolved spectroscopy for in-situ
17
18 610 estimation of concentration and particle size in colloidal suspensions", *Analytical and bioanalytical chemistry*, **409**, 30
19
20 611 (2017).
21
22 612 32. B. Igne, S. Talwar, H. Feng, J.K. Drennen and C.A. Anderson, "Near-Infrared Spatially Resolved Spectroscopy for
23
24 613 Tablet Quality Determination", *Journal of pharmaceutical sciences*, **104**, 12 (2015).
25
26 614 33. M. Hanafi and E.M. Qannari, "Nouvelles propriétés de l'analyse en composantes communes et poids spécifiques",
27
28 615 *Journal de la Société Française de Statistique*, **149**, 2 (2008).
29
30 616 34. E.M. Qannari, I. Wakeling, P. Courcoux and H.J. MacFie, "Defining the underlying sensory dimensions", *Food*
31
32 617 *Quality and Preference*, **11**, 1-2 (2000).
33
34 618 35. E.M. Qannari, P. Courcoux and E. Vigneau, "Common components and specific weights analysis performed on
35
36 619 preference data", *Food Quality and Preference*, **12**, 5-7 (2001).
37
38 620 36. M. Hanafi, G. Mazerolles, E. Dufour and E.M. Qannari, "Common components and specific weight analysis and
39
40 621 multiple co-inertia analysis applied to the coupling of several measurement techniques", *J. Chemometrics*, **20**, 5
41
42 622 (2006).
43
44 623 37. F. Ammari, L. Bassel, C. Ferrier, D. Lacanette, R. Chapoulie and B. Bousquet, "Multi-block analysis coupled to laser-
45
46 624 induced breakdown spectroscopy for sorting geological materials from caves", *Talanta*, **159** (2016).
47
48
49
50
51
52
53
54
55
56

- 1
2
3 625 38. A. Kulmyrzaev, É. Dufour, Y. Noël, M. Hanafi, R. Karoui, E.M. Qannari and G. Mazerolles, "Investigation at the
4
5 626 molecular level of soft cheese quality and ripening by infrared and fluorescence spectroscopies and chemometrics—
6
7 627 relationships with rheology properties", *International Dairy Journal*, **15**, 6-9 (2005).
8
9
10 628 39. J. Pram Nielsen, D. Bertrand, E. Micklander, P. Courcoux and L. Munck, "Study of NIR spectra, particle size
11
12 629 distributions and chemical parameters of wheat flours: a multi-way approach", *Journal of Near Infrared Spectroscopy*,
13
14 630 **9** (2001).
15
16 631 40. M. Rey-Bayle, R. Bendoula, S. Henrot, K. Lamiri, F. Baco-Antoniali, N. Caillol, A. Gobrecht and J.-M. Roger,
17
18 632 "Potential of vis-NIR spectroscopy to monitor the silica precipitation reaction", *Analytical and bioanalytical chemistry*,
19
20 633 **409**, 3 (2017).
21
22 634 41. I. Boudimbou, *Mécanismes élémentaires de dispersion de charges de silice dans une matrice élastomère*, Paris
23
24 635 (2011).
25
26 636 42. Deka MOUSSA RAGUEH, *Filtration de silices précipitées: mise en évidence des relations entre propriétés*
27
28 637 *macroscopiques et échelles locales caractéristiques dans les dépôts*, Toulouse (2011).
29
30 638 43. A. Fukumoto, C. Dalmazzone, D. Frot, L. Barré and C. Noik, "Investigation on Physical Properties and Morphologies
31
32 639 of Microemulsions formed with Sodium Dodecyl Benzenesulfonate, Isobutanol, Brine, and Decane, Using Several
33
34 640 Experimental Techniques", *Energy Fuels*, **30**, 6 (2016).
35
36 641 44. s. donertas, "Core Flooding Sytem", <http://www.corelab.com/sanchez/enhanced-oil-recovery/cfs-700>.
37
38 642 45. S. Shaddel, M. Hemmati, E. Zamanian and N. Moharrami, "Core flood studies to evaluate efficiency of oil recovery
39
40 643 by low salinity water flooding as a secondary recovery process", *Journal of Petroleum Science and Technology*, **4**
41
42 644 (2014).
43
44 645 46. E. Dubin, M. Spiteri, A.-S. Dumas, J. Ginet, M. Lees and D.N. Rutledge, "Common components and specific weights
45
46 646 analysis: A tool for metabolomic data pre-processing", *Chemometrics and Intelligent Laboratory Systems*, **150** (2016).
47
48 647 47. D.N. Rutledge, *Extensions of Common Component and Specific Weight Analysis for applications in Chemometrics*,
49
50 648 AgroParisTech (2013).
51
52
53
54
55
56
57
58
59
60

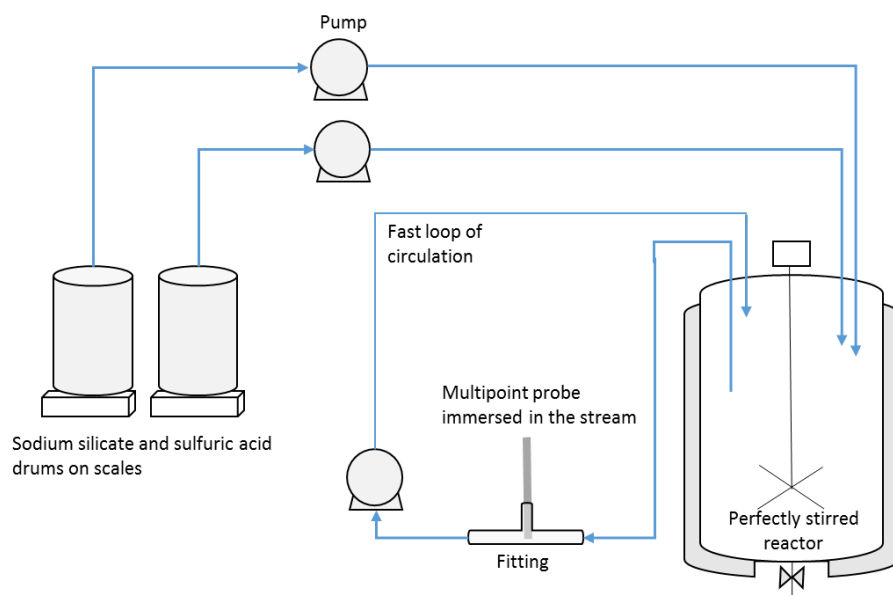
- 1
2
3 649 48. H. Büning-Pfaue, "Analysis of water in food by near infrared spectroscopy", *Food Chemistry*, **82**, 1 (2003).
4
5 650 49. J. Schlomach and M. Kind, "Investigations on the semi-batch precipitation of silica", *Journal of Colloid and*
6
7 651 *Interface Science*, **277**, 2 (2004).
8
9 652 50. J. Baldyga, M. Jasinska, K. Jodko and P. Petelski, *Precipitation of amorphous colloidal silica from aqueous*
10
11 653 *solutions* (2012).
12
13 654 51. J. Gregory, "Monitoring particle aggregation processes", *Advances in colloid and interface science*, **147-148**
14
15 655 (2009).
16
17 656 52. K. Quarch, E. Durand, C. Schilde, A. Kwade and M. Kind, "Mechanical fragmentation of precipitated silica
18
19 657 aggregates", *Chemical Engineering Research and Design*, **88**, 12 (2010).
20
21 658 53. S. Musić, N. Filipović-Vinceković and L. Sekovanić, "Precipitation of amorphous SiO₂ particles and their
22
23 659 properties", *Braz. J. Chem. Eng.*, **28**, 1 (2011).
24
25 660 54. K.D. Dahm and D.J. Dahm, "Separating the Effects of Scatter and Absorption Using the Representative Layer",
26
27 661 *Journal of Near Infrared Spectroscopy*, **21**, 5 (2013).
28
29 662 55. R. Steponavičius and S.N. Thennadil, "Extraction of chemical information of suspensions using radiative transfer
30
31 663 theory to remove multiple scattering effects: application to a model multicomponent system", *Analytical chemistry*,
32
33 664 **83**, 6 (2011).
34
35 665 56. E. Herremans, E. Bongaers, P. Estrade, E. Gondek, M. Hertog, E. Jakubczyk, N. Nguyen Do Trong, A. Rizzolo, W.
36
37 666 Saeys, L. Spinelli, A. Torricelli, M. Vanoli, P. Verboven and B. Nicolai, "Microstructure–texture relationships of aerated
38
39 667 sugar gels: Novel measurement techniques for analysis and control", *Innovative Food Science & Emerging*
40
41 668 *Technologies*, **18** (2013).
42
43 669 57. R. XU, *Particle characterization: light scattering methods*. Kluwer academic publishers, Miami (2002).
44
45
46
47
48
49
50
51
52
53
54
55
56
57
58
59
60

1
2
3
4
5
6
7
8
9
10
11
12
13
14
15
16
17
18
19
20
21
22
23
24
25
26
27
28
29
30
31
32
33
34
35
36
37
38
39
40
41
42
43
44
45
46
47
48
49
50
51
52
53
54
55
56
57
58
59
60



Multi-angle probe diagram (Sam-Flex, Indatech)

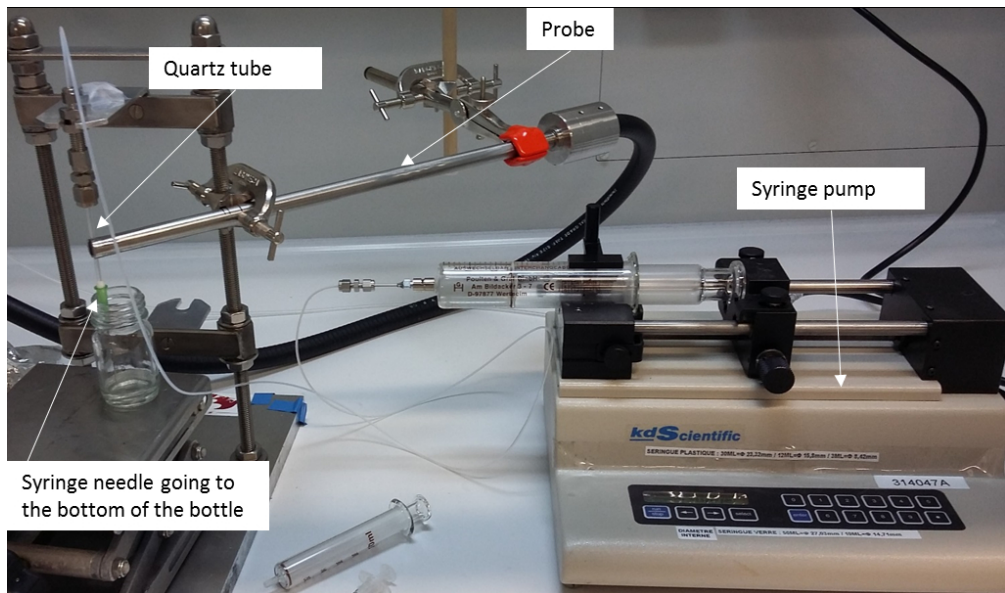
81x51mm (150 x 150 DPI)



Experimental set up

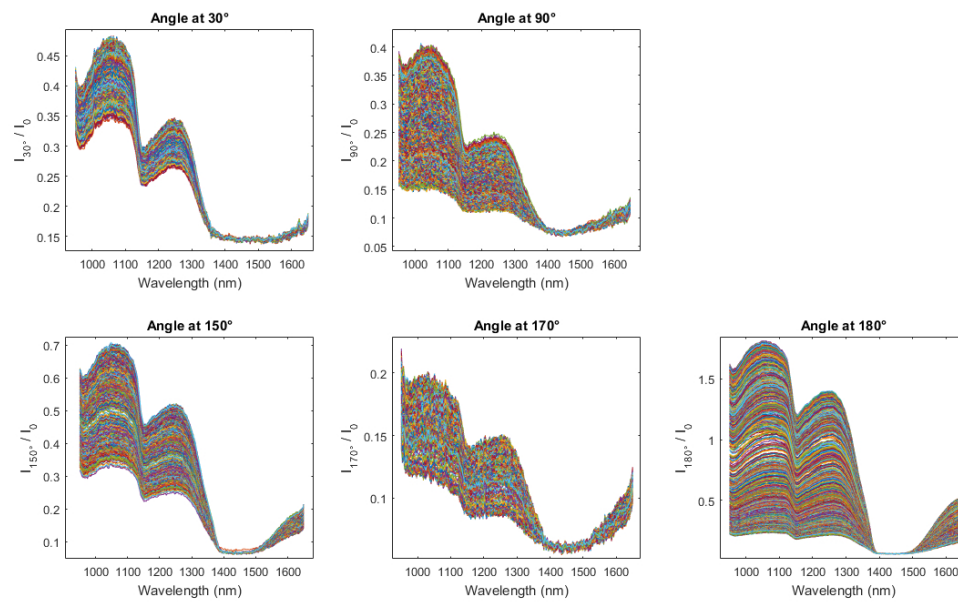
192x122mm (150 x 150 DPI)

1
2
3
4
5
6
7
8
9
10
11
12
13
14
15
16
17
18
19
20
21
22
23
24
25
26
27
28
29
30
31
32
33
34
35
36
37
38
39
40
41
42
43
44
45
46
47
48
49
50
51
52
53
54
55
56
57
58
59
60



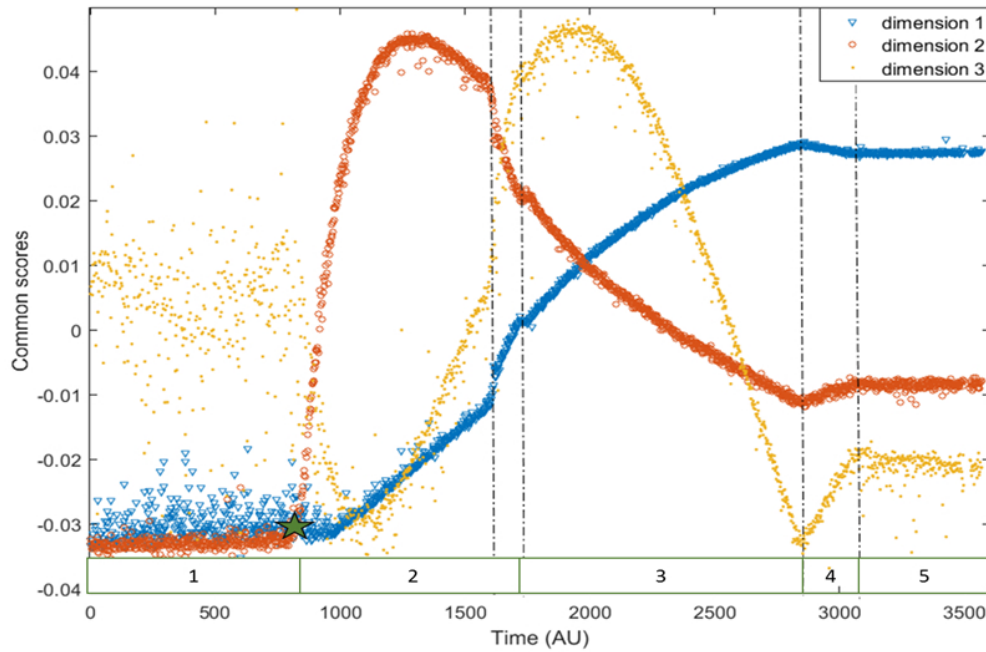
Photograph of the experimental set up

173x101mm (150 x 150 DPI)



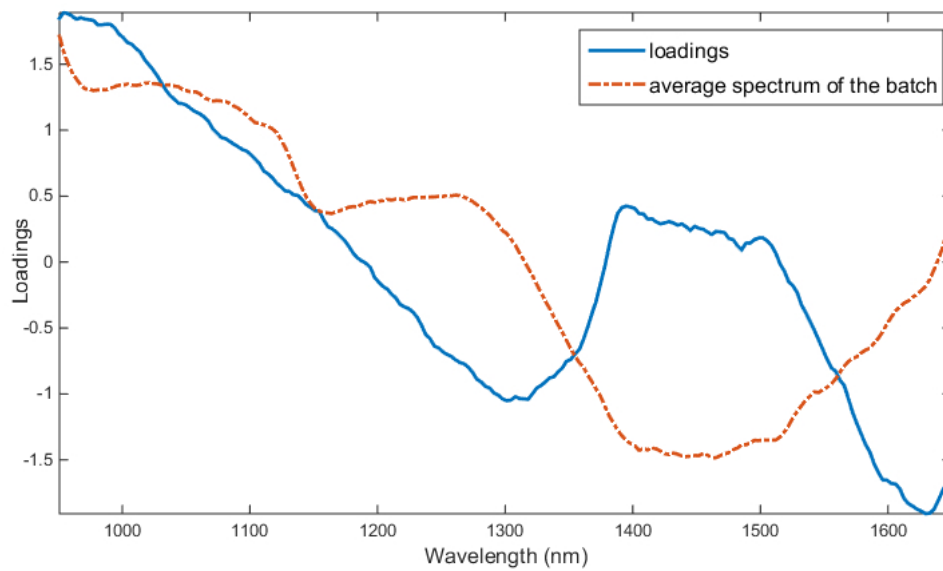
Spectra I/I_0 at the five angles throughout the batch

290x182mm (96 x 96 DPI)



Common scores for three common dimensions according to time. The dotted lines correspond to the modifications of the process, the star and the numbered strips correspond to product evolutions

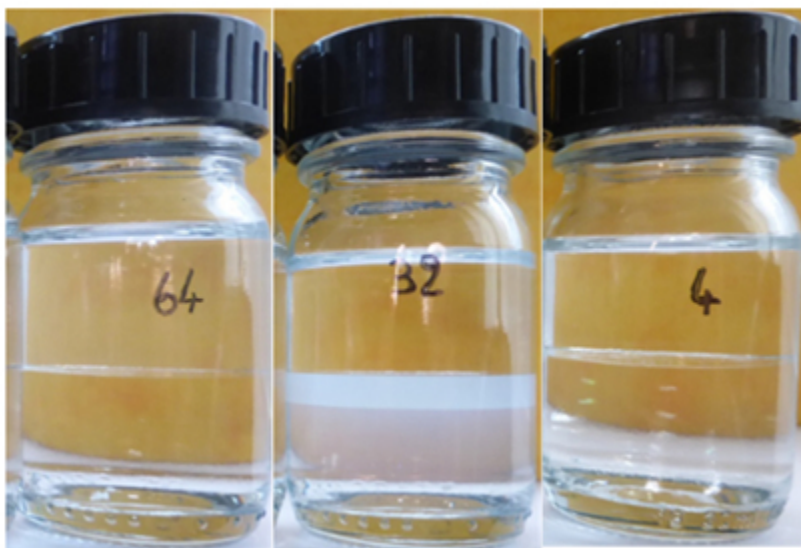
135x89mm (150 x 150 DPI)



Average spectrum of the batch and loadings obtained for the angle 170° in the second dimension

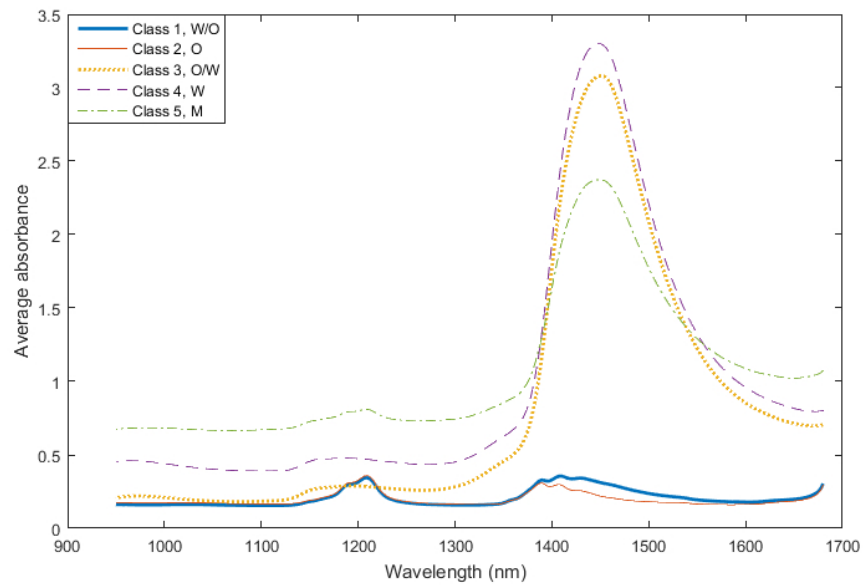
197x143mm (96 x 96 DPI)

1
2
3
4
5
6
7
8
9
10
11
12
13
14
15
16
17
18
19
20
21
22
23
24
25
26
27
28
29
30
31
32
33
34
35
36
37
38
39
40
41
42
43
44
45
46
47
48
49
50
51
52
53
54
55
56
57
58
59
60



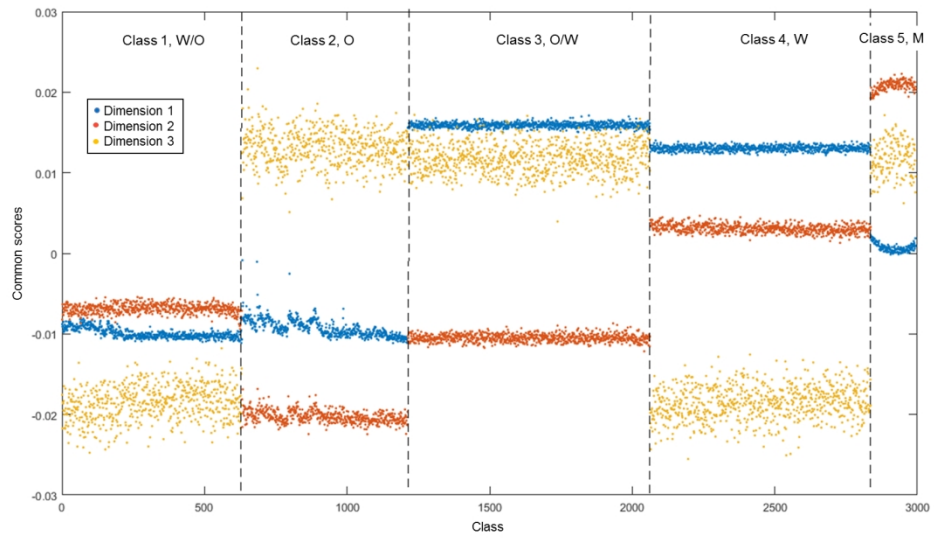
Photograph of the 3 samples for the micro-emulsion application

74x50mm (150 x 150 DPI)



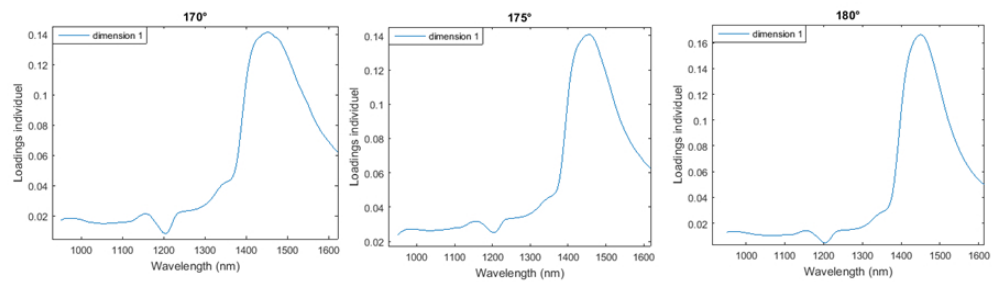
Mean absorption spectra of classes

212x134mm (96 x 96 DPI)



Common scores for three common dimensions according to the classes

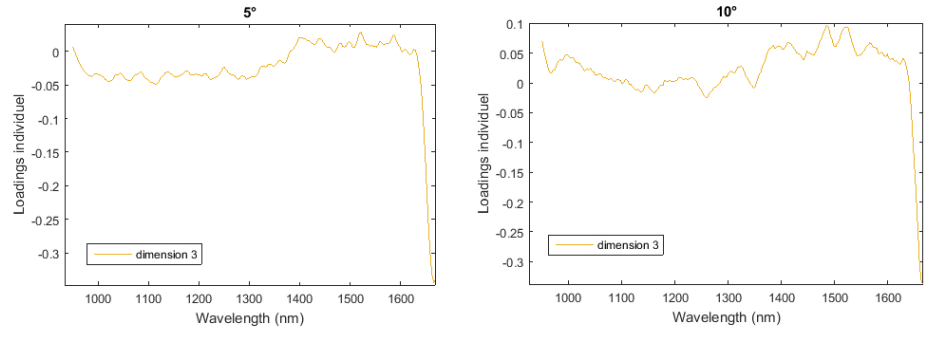
306x177mm (150 x 150 DPI)



Individual loadings of transmission angles to the first dimension

240x70mm (96 x 96 DPI)

1
2
3
4
5
6
7
8
9
10
11
12
13
14
15
16
17
18
19
20
21
22
23
24
25
26
27
28
29
30
31
32
33
34
35
36
37
38
39
40
41
42
43
44
45
46
47
48
49
50
51
52
53
54
55
56
57
58
59
60



Individual loadings of angles at 5° and 10° of the third dimension
278x130mm (96 x 96 DPI)